Current Optics and Photonics
Vol. 2, No. 4, August 2018, pp. 361-367

ISSN: 2508-7266(Print) / ISSN: 2508-7274(Online)
DOI: https://doi.org/10.3807/COPP.2018.2.4.361

Plasmon Assisted Deep-ultraviolet Pulse Generation from Amorphous Silicon Dioxide in Nano-aperture

Hyunsu Lee[1], Heesang Ahn[1], Kyujung Kim[1,2], and Seungchul Kim[1,2]*

[1]*Department of Cogno-Mechatronics Engineering, Pusan National University, Busan 46241, Korea*
[2]*Department of Optics and Mechatronics Engineering, Pusan National University, Busan 46241, Korea*

(Received June 26, 2018 : revised July 23, 2018 : accepted July 25, 2018)

Ultrafast deep-ultraviolet (DUV) pulse generation from the subwavelength aperture of a plasmonic waveguide was investigated. The plasmonic nanofocusing of near-infrared (NIR) pulses was exploited to enhance DUV photoemission of surface third harmonic generation (STHG) at the amorphous SiO_2 dielectric. The generated DUV pulses which are successfully made from a nano-aperture using 10 fs NIR pulses have a spectral bandwidth of 13 nm at a carrier wavelength of 266 nm. This method is applicable for tip-based ultrafast UV laser spectroscopy of nanostructures or biomolecules.

Keywords : Local field enhancement, Ultrafast deep-ultraviolet, Surface plasmon, Surface third harmonic generation
OCIS codes : (190.4350) Nonlinear optics at surfaces; (250.5403) Plasmonics; (320.7090) Ultrafast lasers

I. INTRODUCTION

An ultrafast ultraviolet pulse having a pulse duration of a few femtoseconds has potential in the area of investigating electron relaxation in atoms [1], plasmonic behavior [2] or ultrafast molecular formation [3]. For modifying the ultrafast electron dynamics in the valence shell of atoms and molecules, few-cycle light pulses in the DUV are essential in ultrafast laser experiments [4]. Since the DUV has higher photon energy than visible light, it is useful for triggering and observing the reactions of DNA or bio-molecules [5-7]. For instance, DUV resonance Raman (DUVRR) spectroscopy has been used for protein structural characterization at all stages of fibrillation [8]. In such an application, the smaller beam size of the DUV excitation source is desirable for minimizing background signal in observing inelastic scattering from such molecules.

Surface plasmons (SP) have attracted increasing attention in the last decades, mainly as these electromagnetic waves propagating at the interface between a metal and a dielectric are spatially confined beyond the diffraction limit [13, 21, 23-25]. Guiding SP energy into the small, nano-metric volume has been reported by previous investigations using a planar metallic tip [14] or a 2-dimensional V-groove [15]. The plasmonic focusing readily achieved the concentration NIR/visible pulse into the subwavelength sized spot at the metallic tip [9, 10]. However, the subwavelength guidance of high-frequency electromagnetic DUV is challenging because of low plasmonic coupling efficiency in the DUV spectral region for most metals. The nanoscale plasmonic ultraviolet laser was demonstrated by exploiting the nanowire, but it generates a monochromatic laser [11]. A plasmonic Au bow-tie antenna can be used to make a third harmonic pulse at a carrier wavelength of 400 nm by multiphoton resonances with the d-band transitions of Au, but this method can not reach into DUV frequency due to the band structure of Au. Nanoscale high harmonic generation was also demonstrated by injecting a noble gas onto the microfunnel structure for generating short wavelength light source, but its conversion efficiency is too low to be applicable in many biological experiments [18, 19]. The metal-sapphire crystalline nanofunnel was recently reported to improve the efficiency of plasmon-assisted high harmonic generation, but no other nonlinear

*Corresponding author: s.kim@pusan.ac.kr, ORCID 0000-0002-6765-2471
Color versions of one or more of the figures in this paper are available online.

effects have been discussed on such type of metal-dielectric nanostructures [22].

Here, we investigated a method for generating DUV pulses, applicable for nanophotonic applications, having a carrier wavelength of 266 nm and a repetition rate of 75 MHz. The waveguide is embedded on the microcantilever as shown in Fig. 1(a). The suggested 3-dimensional tapered waveguide as shown in Fig. 1 is designed for generating high field enhancement at the exit aperture of the waveguide where the NIR pulse is mostly blocked. In light of plasmonic-photon coupling, a planar V-groove is a beneficial structure when two dimensional focusing is considered. However, a cone-like structure is more desirable to concentrate all plasmonic energy into one localized area. As for the compromised design, the elliptical funnel structure has suggested in this investigation and the numerical simulations also showed that the compromised design has higher intensity enhancement thatnother type of focusing design. Similar funnel structures were previously reported for inducing high harmonic generation, but our method uses the thickness-controlled amorphous dielectric to make the local electric field only at the surface for generating surface third harmonics [18-20].

The DUV pulse is generated by a surface-enhanced third harmonic generation (STHG), frequency up-conversion process of the NIR femtosecond pulse. STHG is known as an interesting nonlinear process which only takes place at the interface of two dielectrics, implying less consideration in phase matching of generated DUV pulse. However, the relative efficiency of STHG is weaker than that of bulk third harmonic generation. Therefore, plasmonic nanofocusing in the 3-dimensional metallic waveguide was adopted to increase the STHG efficiency. Geometrically, the elliptical shaped funnel structure was considered to get more plasmonic field enhancement than the circular funnel. The thickness of the amorphous silicon dielectric layer was also controlled to have higher field enhancement at the tip of the nano-aperture. From our study, the efficiency of plasmonic STHG was increased to be 10^5 times theoretically and 10^2 times experimentally. The suggested light source will enable new experimental schemes in the field of nanophotonics such as ultrafast time-resolved spectroscopy, near-field DUV resonant Raman spectroscopy and high spatiotemporal microscopy of the bio-molecular specimen.

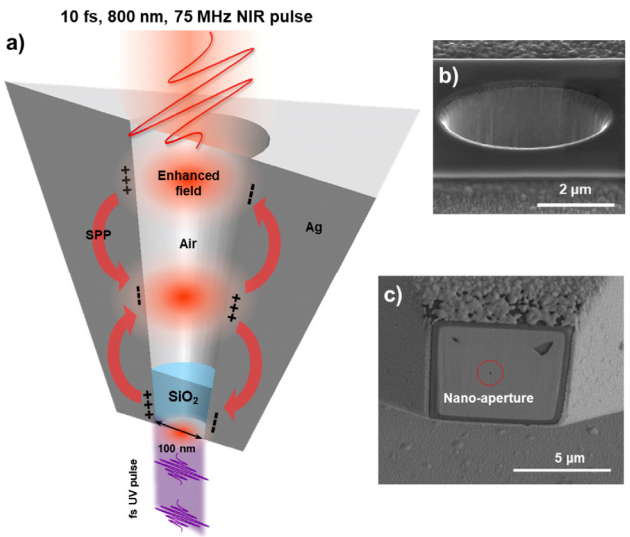

FIG. 1. (a) Schematic diagram of plasmonically enhanced generation of ultrafast DUV pulse emitting from the subwavelength spot of hybrid 3-dimensional waveguide. The waveguide is embedded on the micro-cantilever for the purpose of scanning with high spatial selectivity. The NIR femtosecond pulse is excited on the micro sized aperture and transformed into surface plasmon. This surface plasmon is propagated to the tapered end and formed strong local field at the air-SiO_2 interface, enabling STHG at the nano aperture. (b) Scanning electron microscope image of input aperture where femtosecond laser is illuminated. (c) Scanning electron microscope image of exit aperture where generated third harmonic is emitted.

II. NUMERICAL SIMULATION

STHG is induced by focusing light on the interface of two different dielectrics due to the discontinuity of third order susceptibility at the interface [16]. One advantage of STHG is that the generated third harmonic pulse has negligible chromatic dispersion since it is only created the at the surface of dielectric [12]. The magnitude of third-order susceptibility, χ^3 at the interface is at least three orders of magnitude larger than the values of the internal dielectric medium. Nevertheless, the overall efficiency of STHG is lower than those from conventional methods using a thick third-harmonic crystal due to the short interacting length/volume. Therefore, the higher pumping intensity is required at the interface to increase STHG efficiency because the efficiency of the third harmonic process is linearly proportional to the cube of the intensity at the interface. This brings the field enhancement using surface plasmon polaritons (SPPs) which is capable of enormously enhancing the incident laser intensity.

The device consists of two different sections which have air-filled and SiO_2 filled regions. When the NIR femtosecond pulse is focused through the hollow tapered Ag waveguide, SPPs are induced along the interface between air and Ag. The generated SPPs propagate inside the SiO_2 layer and form high field enhancement at the bottom end of the SiO_2-air interface. The STHG is generated at this interface with an increased efficiency which is proportional to the cube of intensity enhancement of the fundamental laser pulse. The third harmonics are only produced at the interface between SiO_2 and air so the mode area of the DUV beam can be reduced down to sub-wavelength scale by modifying the area of the exit aperture.

The strong intensity enhancement at the exit aperture is a key function in this scheme of ultrafast DUV generation.

We found that the amount of intensity enhancement is significantly affected by the thickness of SiO_2 as well as by the geometrical shape of the funnel waveguide. As illustrated in Fig. 2(a), the elliptical funnel waveguide can be characterized by five parameters; the ellipticity of the cross-section (r = b/a), the minor diameter of the exit aperture (d), the cone angle defined in the minor-axis plane (θ), and the funnel height (h_1) and thickness of SiO_2 (h_2).

To design the funnel structure, we set all possible geometrical parameters. Each parameter affects the amount of local field enhancement at the exit aperture of the funnel, but it is difficult to get the highest field enhancement by varying parameter values because these parameters generate too many simulation sets, requiring an additional optimization algorithm for getting the maximum field enhancement. For optimizing the intensity enhancement at the exit aperture without a numerical algorithm, the finite-difference-time-domain method was used to calculate Maxwell's equations and we set the maximum and minimum geometrical values with a consideration of fabrication capability. As an excitation source, the femtosecond pulse is assumed to have a center wavelength of 800 nm and bandwidth of 100 nm corresponding to a pulse duration of 10 fs. The wavelength dependent complex dielectric constant of Ag was determined by the modified Debye model. The relative permittivity of the SiO_2 was assumed to be constant at 2.13. The

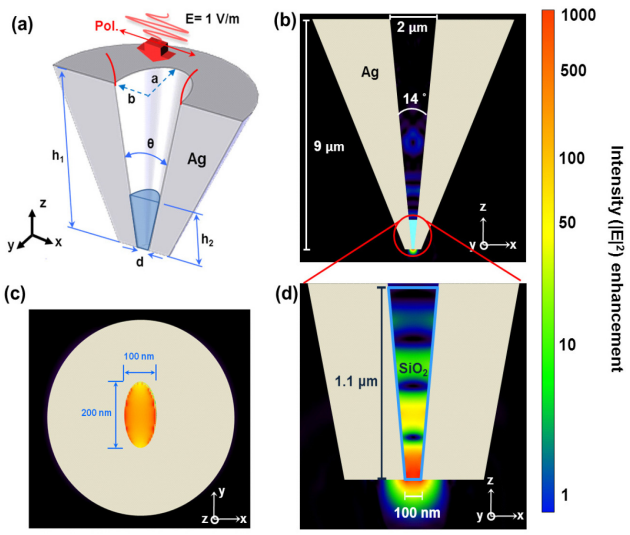

FIG. 2. Finite-difference time-domain calculation results of local field enhancement in waveguide. (a) Geometrical description of waveguide. The polarization direction of incident femtosecond pulse is parallel to the x-y plane denoted as red abbreviation 'pol.' (b) Computed intensity field in the x-z plane (c) Same results in x-y plane. (d) Magnified view near the exit aperture of waveguide. The blue trapezoid in waveguide is filled with the SiO_2. The intensity enhancement factor at exit aperture reaches an intensity enhancement higher than 400 in the whole area. The selected design parameters were h_1 = 9 μm, h_2 = 1.1 μm, d = 100 nm, θ = 14 °, r = 0.5 respectively.

polarization direction of the incident femtosecond pulse is parallel to the minor axis of the elliptical cross-section of waveguide denoted as 'Pol.' in Fig. 2(a). The hexahedral grid of mesh size of 5 nm × 5 nm × 5 nm in size was used for dividing the waveguide structure. The parameters were set to get the maximum enhanced field at the interface between SiO_2 and air for given fabrication constraints. The computation result showed that intensity enhancement more than 400 appeared uniformly at the exit aperture which has an elliptical cross-sectional area of 100 nm (x) × 200 nm (y). The overall intensity enhancement factor on exit aperture is decreased down to ~100 when no SiO_2 layer exists in the metallic funnel. Theoretically, the efficiency of STHG in a partially SiO_2 deposited funnel can be increased by 6.4×10^7 including reduction of the effective area of the third harmonic process. The chosen value for the geometrical parameters were d = 100 nm, θ = 14 °, h_1 = 9 μm, h_2 = 1.1 μm and r = 0.5. The ellipticity was set at 0.5 to reduce computational conditions in this consideration. It is known that plasmonic focusing takes place efficiently in the V-groove structure when the polarization of excited light is orthogonal to the V-groove surface, but the plasmonic focusing is not generated at the other polarization condition of the light. In light of plasmonic focusing in the V-groove, the plasmonic focusing in the elliptical funnel structure is more efficient than for the circular shaped funnel structure. The tapered rectangular structure is also a good candidate for plasmonic focusing, but we found that the fabricated tapered rectangular structure shows more surface roughness during the focused ion beam milling process since we fabricated the funnel structure in a sequential milling process like a 3D printing process.

The numerical simulation results revealed that the temporal shape of enhanced NIR pulse at the exit aperture has no significant dispersions for a 10 fs pulse, corresponding to the pulse duration of 11.6 fs as depicted in Fig. 3(a). The total propagation length of the SPP is less than 10 μm; thereby frequency dependent dispersions do not affect the temporal shape of the enhanced NIR pulse. The enhanced electric field at the exit aperture is slightly broadened due to the inhomogeneous plasmonic dephasing effect.

STHG does not experience significant pulse broadening by phase velocity mismatching. In electric field calculations, the plasmonic ring-down oscillation was observed at the tail of the enhanced NIR pulse, but it does not much elongate the pulse width of the DUV pulse. From this numerical analysis, the DUV pulse emitting from the exit aperture can be regarded as a Fourier transform limited pulse, having no significant broadening or distortion of the pulse shape.

In most plasmonic structures, the height of the waveguide and the tapered angle are related to the coupling efficiency of NIR pulse into the SPP and to the propagation loss of the SPP. However, the intensity enhancement of our waveguide is very sensitive to both the size of the exit aperture and the thickness of the SiO_2 layer. When the minor axis diameter of the exit aperture is smaller than 100 nm, most

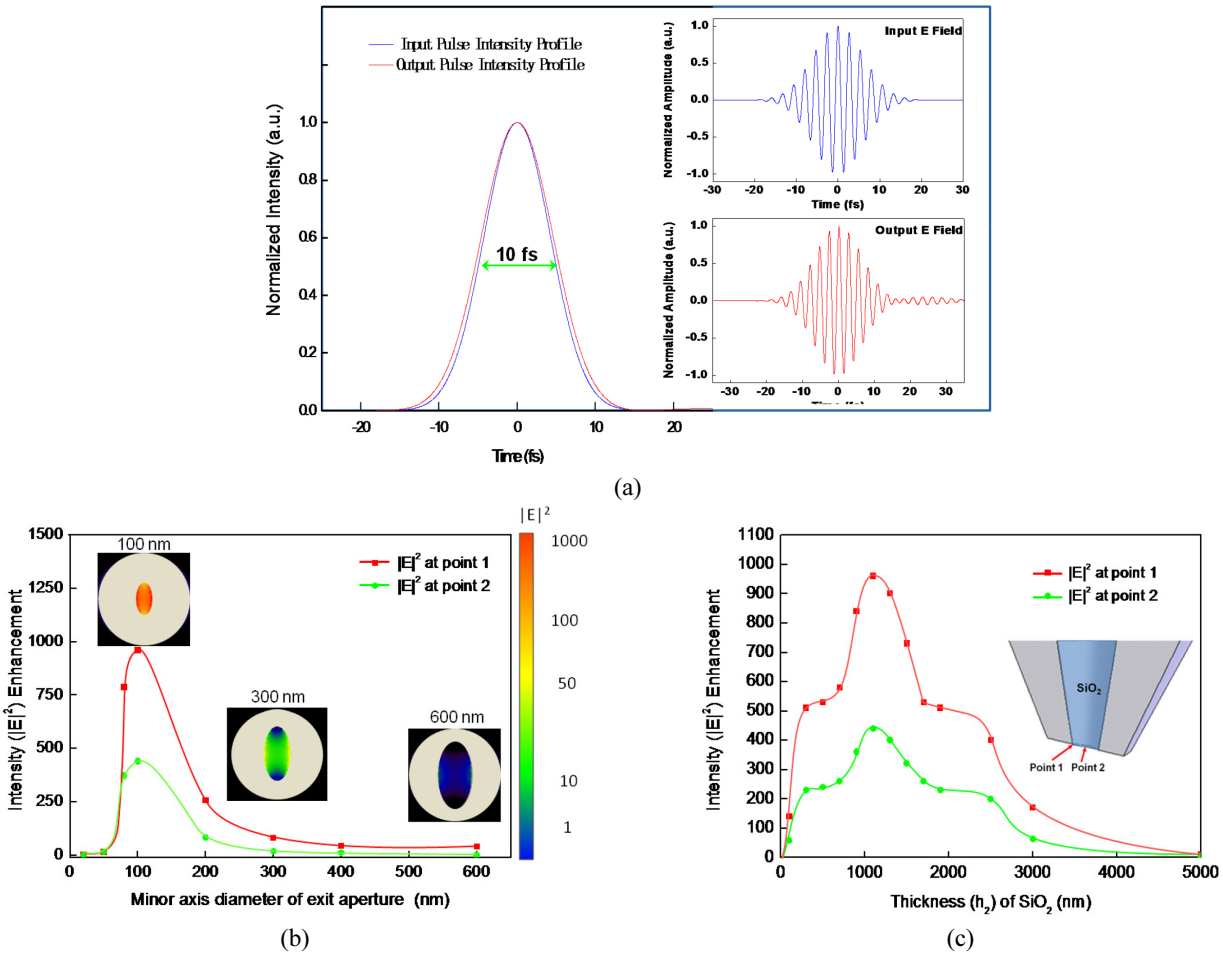

FIG. 3. (a) Temporal characteristic of enhanced pulse at exit aperture. Inset shows normalized electric fields of both input pulse and enhanced pulse. (b) Effect of exit aperture size to the intensity enhancement of NIR pulse. Three insets show the 2-dimensional field distribution of transverse electric field with different sizes of exit. Too small aperture blocks in forming local field at the tip, but relatively large aperture prevents the concentration of surface plasmons (c) Variation of intensity enhancement for the thickness of SiO_2 inside waveguide. 1.1 μm thick SiO_2 layer showed highest field enhancement at the air-SiO_2 interface.

SPPs have begun to decay or have been reflected before reaching the exit aperture, resulting in less intensity enhancement. On the contrary, the aperture size larger than 100 nm in minor axis degrades the concentration, which also induces less intensity enhancement as shown in Fig. 3(b).

The SiO_2 layer inside a tapered waveguide performs not only by inducing STHG by forming the interface with air but also by concentrating SPP energy into the exit aperture as calculated in Fig. 3(c). For the case of the tapered waveguide without an SiO_2 layer, the enhanced field is located inward of the waveguide causing no intensity enhancement at the exit aperture, but the enhanced fields are located inside of the funnel structure. We expect that the SiO_2 layer induced reduction of phase and group velocities in plasmonic propagation because of higher refractive index, leading to further concentration of SPP into the exit aperture. However, it is interesting to note that a thicker SiO_2 layer breaks the coupling condition and induces a loss in SPP build-up which requires further theoretical investigation. To design maximized intensity enhancement at the tip, two different points (point 1 and point 2 as depicted in Fig. 3(c)) are defined. The intensity enhancement at these two points had the same tendency when the thickness of the SiO_2 layer was varied. The intensity enhancement at point 1 is two times higher than that of point 2 which means 8 times different efficiency of generated STHG should be considered for spatial intensity distribution of generated STHG.

III. EXPERIMENTS

Figure 4 shows a scanning electron microscope image of the ultrafast DUV beaming probe fabricated on the commercial cantilever (NASCATEC, NST-SNOM-WAP). The depositing of a Pt layer inside a hollow tip of the cantilever using a focused ion beam (FIB) forms a 2-dimensional square having size 5 μm × 5 μm. After that,

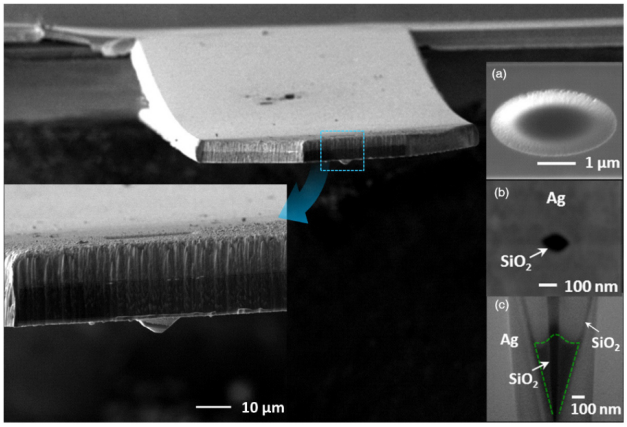

FIG. 4. Scanning electron microscope (SEM) image of the plasmonic waveguide for generating ultrafast DUV pulse on the tip of cantilever. (a) Inlet aperture of waveguide in the view from top. (b) Magnified image of exit aperture on the tip on the cantilever. (c) Magnified, cross-sectional view cut along the major axis of the ellipsoidal profiles of the waveguide. The SEM image shows the undesirable deposition of SiO_2 on the wall with a thickness of ~10 nm as well as deposited SiO_2 layer with a thickness of ~700 nm from the tip of waveguide.

a 10-μm silver layer was deposited on the cantilever by e-beam evaporation. We verified that the surface roughness of the fabricated waveguide is significantly affected by the roughness of the deposited silver surface. The roughness of the waveguide should be reduced to protect the loss of propagating SPP. For that, deposition of a 300-nm thick Pt layer by FIB proceeded to improve the surface roughness of the waveguide down to 10 nm. The designed elliptical profile was drilled onto the Ag layer by FIB milling. Specifically, the whole 3-D elliptical waveguide's inner void was divided into a total of 31 horizontally flat laminates with each being etched in sequence one by one with a ~300 nm depth from the inlet to the exit aperture. By a focused electron beam method, selective deposition of an SiO_2 layer with a thickness of ~700 nm was achieved. Finally, the bottom surface of the tip was polished from the outside until the exit aperture came to have a 100 nm diameter in the minor axis direction. A precise milling process of a focused ion beam enables the exact control of the size of exit aperture with nanometer precision.

For the experimental validation, a Ti:sapphire femtosecond pulse having a pulse duration of 10 fs, center wavelength of 800 nm and repetition rate of 75 MHz was used with precise control of dispersion. The NIR pulses were focused via an aspheric lens to a 5 μm diameter spot on the inlet aperture whose elliptical major and minor diameters was 4.4 μm and 2.2 μm, respectively. The focused femtosecond laser intensity has a peak intensity of 10^{10} Wcm^{-2}, preventing thermal damage to the metallic funnel structure.

To measure the DUV pulse emitted out of the exit aperture, a high sensitivity pre-amplified SiC UV photodiode (Sglux, TOCON_nano) was used with the UV bandpass

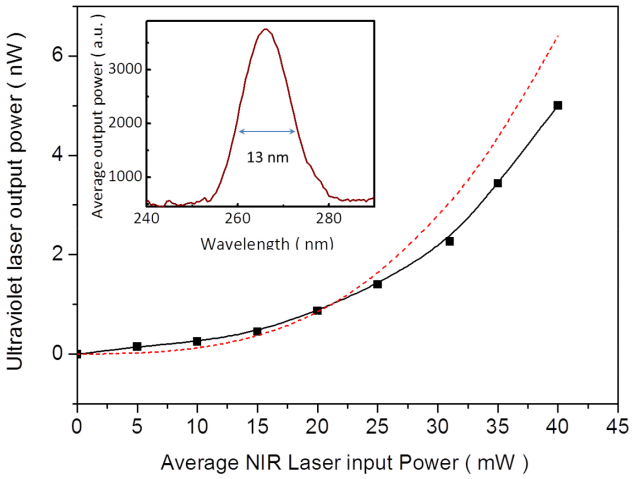

FIG. 5. Power relation between the emitted DUV light and input femtosecond NIR pulse laser. The out power of DUV pulses is proportional to the third power of input femtosecond laser. Upper inset shows measured DUV spectrum which has a full-width half-maximum bandwidth of 13 nm at center wavelength of 266 nm.

filter (eSource Optics, 12260FBB). The UV bandpass filter having an FWHM transmission bandwidth range from 240 nm to 280 nm mostly blocks the NIR pulse. The UV photodiode was located at a distance of 30 mm from the exit aperture, and the UV filter is inserted in front of the photodiode. Figure 5 shows the power ratio between the input NIR pulse laser and the generated UV pulse. The measured power of the DUV pulse is proportional to the third power of incident intensity, (I^3) of the NIR pulse. The conversion efficiency was found to be on the level of 10^{-7} which is 10^2 times higher than bulk STHG on the SiO_2 substrate with the same intensity [16]. The difference between theoretical and experimental third harmonic efficiency is attributed to the undesirable deposition of SiO_2 particles on the inner wall of the whole metallic waveguide during the focused e-beam deposition process, and surface roughness that was not considered in the theoretical calculation. We also verified that the deposited SiO_2 layer has a thickness of ~700 nanometers on the inner side of the waveguide which is not the optimal thickness to get the highest intensity enhancement.

For analyzing the spectrum of the DUV pulse, a broad-band UV/VIS spectrometer (Avantes, Avaspec-2048) was used with UV bandpass filter. The full-width half-maximum bandwidth spectrum was measured as 47 THz, having a Gaussian distribution. This bandwidth is the same as the bandwidth of the incident NIR pulse, meaning no sideband reduction of frequency in the third harmonic process. The autocorrelation of the DUV pulse for estimating pulse duration was not within the scope of the current investigation due to the critical dispersion management of the DUV pulse during the autocorrelation technique. It is predictable that the enhanced femtosecond pulse at the exit aperture

has little dispersion which enables the DUV pulse to be a Fourier-transform limited pulse. Therefore, the DUV pulse directly has a pulse duration of 8 fs without any dispersion compensation scheme. In consideration of emitted power and pulse duration, the UV pulse has a peak intensity of 4×10^7 W-cm^{-2} with a frequency of 75 MHz, sufficient for ultrafast spectroscopic observation [17]. One of the essential characteristics of the nanophotonic tool is the direct illumination of ultrafast light onto the target without an additional delivery system, keeping a short ultrafast DUV pulse.

The spatial distribution of the generated DUV pulse depends on the wave vector of the enhanced femtosecond pulse at the exit aperture. The numerical calculation showed that the normal component of the wave vector which is perpendicular to the surface of the exit aperture is dominant. The measured divergence angle of the DUV pulse was 9 °, which experimentally substantiates the sub-wavelength pinhole diffraction with the same diameter of exit aperture. The beam divergence angle is measured by scanning the UV photodetector laterally when the distance between the detector and the nano-tip is fixed. After measuring the DUV power, the full-width half-maximum DUV light intensity is determined as the divergence angle. Since its effective aperture is smaller than the wavelength of DUV, it is hard to compare the measured angle by applying classical diffraction theory of circular aperture diffraction.

IV. CONCLUSION

In conclusion, we successfully developed broadband DUV pulses, beaming from the probe with modest power of femtosecond pulse laser. This was performed by way of STHG with the assistance of plasmonic nanofocusing of an NIR pulse at the air-SiO_2 interface in the tapered Ag waveguide. The focused NIR pulse was plasmonically enhanced by more than a factor of 400 theoretically, which boosted up the efficiency of STHG at the exit aperture as large as 10^5 theoretically and 10^2 experimentally. Requiring no dispersion compensation techniques and generating a DUV pulse within subwavelength size, the proposed method enables the ultrafast DUV source development with a repetition rate of 75 MHz emitting from the sub-wavelength aperture of the funnel-like nanostructure. This has the potential to be a breakthrough in the area of ultrafast time-resolved spectroscopy, photo-electron emission microscopy, laser-assisted nano-biology, and possibly UV based near-field resonant Raman spectroscopy.

ACKNOWLEDGMENT

This work was supported by a 2-Year Research Grant of Pusan National University.

REFERENCES

1. W. A. Tisdale, K. J. Williams, B. A. Timp, D. J. Norris, E. S. Aydil, and X.-Y. Zhu, "Hot-electron transfer from semiconductor," Science **328**, 1543-1547 (2010).
2. M. I. Stockman, M. F. Kling, U. Kleineberg, and F. Krausz, "Attosecond nanoplasmonic-field microscope," Nat. Photon. **1**, 539-544 (2007).
3. J. Li, Z. Liu, C. Tan, X. Guo, L. Wang, A. Sancar, and D. Zhong, "Dynamics and mechanism of repair of ultraviolet-induced (6-4) photoproduct by photolyase," Nature **466**, 887-891 (2010).
4. F. Reiter, U. Graf, M. Schultze, W. Schweinberger, H. Schröder, N. Karpowicz, A. M. Azzeer, R. Kienberger, F. Krausz, and E. Goulielmakis, "Generation of sub-3 fs pulses in the deep ultraviolet," Opt. Lett. **35**, 2248-2250 (2010).
5. W. J. Schreier, T. E. Schrader, F. O. Koller, P. Gilch, C. E. Crespo-Hernández, V. N. Swaminathan, T. Carell, W. Zinth, and B. Kohler, "Thymine dimerization in DNA is an ultrafast photoreaction," Science **315**, 625-629 (2007).
6. Y. Liu, B. Tang, H. Shen, S. Zhang, and B. Zhang "Probing ultrafast internal conversion of o-xylene via femtosecond time-resolved photoelectron imaging," Opt. Express **18**, 5791-5801 (2010).
7. O. Geßner, A. M. D. Lee, J. P. Shaffer, H. Reisler, S. V. Levchenko, A. I. Krylov, J. G. Underwood, H. Shi, A. L. L. East, D. M. Wardlaw, E. T. H. Chrysostom, C. C. Hayden, and A. Stolow "Femtosecond multidimensional imaging of a molecular dissociation," Science **311**, 219-222 (2006).
8. M. Xu, V. V. Ermolenkov, V. N. Uversky, and I. K. Lednev, "Hen egg white lysozyme fibrillation: a deep-UV resonance Raman spectroscopic study," J. Biophotonics **1**, 215-229 (2008).
9. M. I. Stockman, "Nanofocusing of optical energy in tapered plasmonic waveguides," Phys. Rev. Lett. **93**, 137404 (2004).
10. A. J. Babadjanyan, N. L. Margaryan, and Kh. V. Nerkararyan, "Superfocusing of surface polaritons in the conical structure," J. Appl. Phys. **87**, 3785-3788 (2000).
11. R. F. Oulton, V. J. Sorger, T. Zentgraf, R.-M. Ma, C. Gladden, L. Dai, G. Bartal, and X. Zhang "Plasmon lasers at deep subwavelength scale," Nature **461**, 629-632 (2009).
12. T. Y. F. Tsang, "Surface-plasmon-enhanced third-harmonic generation in thin silver films," Opt. Lett. **21**, 245-247 (1996).
13. D. K. Gramotnev, "Plasmonics beyond the diffraction limit," Nat. Photon. **4**, 83-91 (2010).
14. V. S. Volkova, and S. I. Bozhevolnyi, "Bend loss for channel plasmon polaritons," Appl. Phys. Lett. **89**, 143108 (2006).
15. E. Verhagen, A. Polman, and L. (Kobus) Kuipers, "Nanofocusing in laterally tapered plasmonic waveguides," Opt. Express **16**, 45-57 (2008).
16. T. Y. F. Tsang, "Optical third-harmonic generation at interfaces," Phys. Rev. A **52**, 4116-4125 (1995).
17. C.-H. Tseng, S. Matsika, and T. C. Weinacht, "Two-dimensional ultrafast fourier transform spectroscopy in the deep ultraviolet," Opt. Express **17**, 18788-18793 (2009).
18. I.-Y. Park, S. Kim, J. Choi, D.-H. Lee, Y.-J. Kim, M. F. Kling, M. I. Stockman, and S.-W. Kim, "Plasmonic generation of ultrashort extreme-ultraviolet light pulses," Nat. Photon. **5**, 677-681 (2011).
19. H. Kim, S. Han, Y. W. Kim, S. Kim, and S.-W. Kim,

"Generation of coherent extreme-ultraviolet radiation from bulk sapphire crystal," ACS Photon., **4**, 1627-1632 (2017).
20. I.-Y. Park, J. Choi, D.-H. Lee, S. Han, S. Kim, and S.-W. Kim "Generation of EUV radiation by plasmonic field enhancement using nano-structured bowties and funnel-waveguides," Ann. Phys. **525**, 87-96, (2013).
21. H. Kim, J. Kim, H. An, Y. Lee, G.-Y. Lee, J. Na, K. Park, S. Lee, S.-Y. Lee, B. Lee, and Y. Jeong, "Metallic Fresnel zone plate implemented on an optical fiber facet for super-variable focusing of light," Opt. Express **25**, 30290-30303 (2017).
22. S. Han, H. Kim, Y. W. Kim, Y.-J. Kim, S. Kim, I.-Y. Park, and S.-W. Kim, "High harmonic generation by strongly enhanced femtosecond pulses in metal-sapphire nanostructure waveguide," Nat. Commun. 7, 13105 (2016).
23. H. Kim, S. Y. Lee, S. Koo, J. Kim, K. Park, D. Lee, L. A. Vazquez-Zuniga, N. Park, B. Lee, and Y. Jeong, "Theoretical study on the generation of a low-noise plasmonic hotspot by means of a trench-assisted circular nano-slit," Opt. Express **22**, 26844-26853 (2014).
24. M. Hentsche, T. Utikal, H. Giessen, and M. Lippitz, "Quantitative modeling of the third harmonic emission spectrum of plasmonic nanoantennas," Nano Lett. **12**, 3778-3782 (2012).
25. M. Kauranen and Z. Anatoly, "Nonlinear plasmonics," Nat. Photon. **6**, 737 (2012).